ACS OMEGA

http://pubs.acs.org/journal/acsodf

Article

Adsorption of Mercury on Chlorine-Modified Activated Carbon: Breakthrough Curves and Temperature-Programmed Desorption

Julian Steinhaus,* Christoph Pasel, Christian Bläker, and Dieter Bathen

Cite This: *ACS Omega* 2022, 7, 23833−23841

Read Online

ACCESS | Metrics & More | Article Recommendations | Supporting Information

ABSTRACT: The adsorption of elemental mercury (Hg^0) on activated carbons modified with 0.2, 0.6, and 1 M HCl is systematically examined. Breakthrough curves are measured, and coupled adsorption and desorption experiments with temperature-programmed desorption (TPD) are performed. The experiments show that impregnation with HCl produces surface-bound chlorine, which significantly increases the capacity of activated carbons for mercury. Physisorptive interactions between elemental mercury and the activated carbon surface dominate on the basic materials. In contrast, on HCl-modified activated carbons, chemisorptive interactions of Hg^0 with surface-bound chlorine lead to a complex involving carbon, chlorine, and mercury. Using TPD, two mechanisms could be identified that yield reaction products with different energetic values. By continuously recording Hg^0 and Hg_{total} concentrations, the formation of Hg^0 and Hg_xCl_2 during desorption of the complexes from the surface could be studied. It is shown that Hg_xCl_2 found in TPD is not present as a solid salt in the pores but is formed by thermal degradation of the mercury chlorine complex on the carbon surface. The mass fraction of Hg measured in TPD which is bound in Hg_xCl_2 depends on the Hg loading of the activated carbons, with a maximum mass fraction of 27%. We propose that an important step in the chemisorptive reaction with increasing mercury loading is the conversion of a $HgCl_2$ complex into a Hg_2Cl_2 complex.

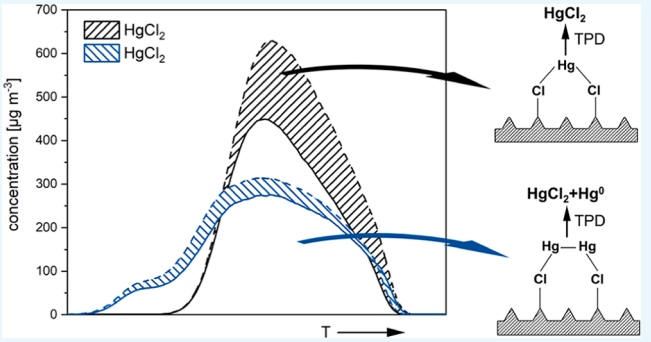

INTRODUCTION

Mercury is a toxic environmental poison that becomes part of a global substance cycle between air, water, and soil and accumulates biologically. For this reason, reducing emissions is a goal of national and international regulations. State of the art is the cleaning of the waste gases of large emitters such as coal power plants by absorption in scrubbers[1−3] or entrained flow adsorbers.[4−7] Small emitter exhaust gases can be treated in a technically and economically efficient way using fixed-bed adsorbers with impregnated[8−16] or nonimpregnated[17−25] activated carbons. A precise knowledge of the adsorption mechanisms is essential for the design of adsorbers and optimization of the operating conditions.

Mercury is emitted during combustion processes in the elemental or oxidized form. Because elemental mercury is present in higher concentrations in the gas phase due to its higher volatility and adsorbs worse than oxidized mercury, only the adsorption of elemental mercury is investigated in this publication. In previous publications,[22,26,27] the physisorptive single-component adsorption of Hg^0, as well as the influence of the coadsorptives water and oxygen, have been presented in detail. As the physisorptive capacity of nonimpregnated activated carbons is very low, impregnated activated carbons are used for chemisorptive separation in technical applications. The adsorbents must have high chemisorptive capacity, fast kinetics, and high thermal stability of the bound mercury. Activated carbons modified with chlorine provide an alternative, which is not yet widely used in industrial applications. Therefore, the following literature analysis exclusively focuses on the chemisorption of elemental mercury on chlorine-modified activated carbons.

Zeng et al.[28] studied the adsorption of Hg^0 on activated carbons impregnated with $ZnCl_2$. They suspected that Hg^0 reacts with a chloride ion to form a mercury chloride species that adsorbs on the surface. Lee et al.[29] modified activated carbon with diluted HCl solution at 70 °C. The mass fraction of chlorine was increased up to 1.73 wt % by impregnation, with a slight decrease in the specific surface area. Adsorption experiments showed high capacities for Hg^0, while scanning electron microscopy−energy dispersive spectroscopy (SEM−EDS) and X-ray photoelectron spectroscopy (XPS) indicated

Received: April 22, 2022
Accepted: June 10, 2022
Published: June 28, 2022

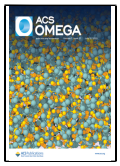

Table 1. Chemical Composition of the Adsorbents

activated carbon	raw material	activation method	ash content	C	S	N	H	O
			[weight % of dry mass]					
AC 01	anthracite	steam	10.7	87.4	0.24	0.32	0.53	0.8
AC 02	coconut shell	steam	2.9	90.4	0.44	0.23	0.51	5.5

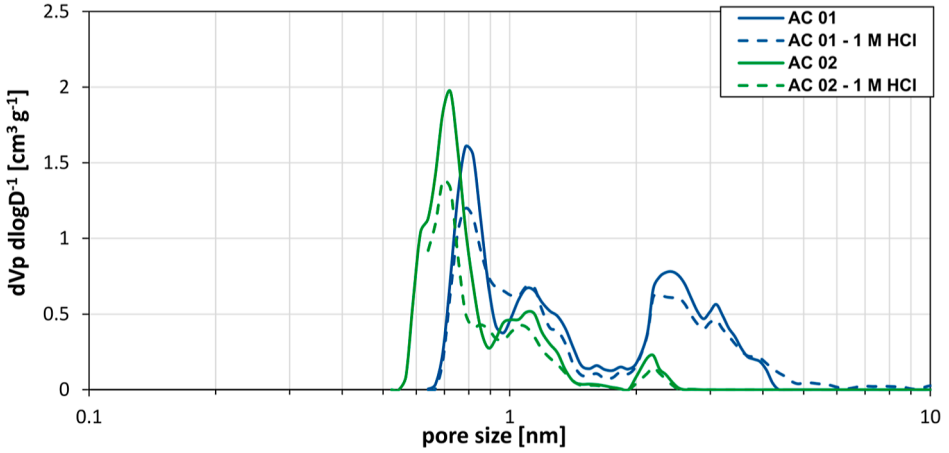

Figure 1. Pore size distribution of basic and HCl-modified activated carbons AC 01 and AC 02.

formation of mercuric chloride on the surface of the activated carbon.

Choi and Lee[30] modified commercial activated carbons with HCl, $FeCl_3$, and $CuCl_2$ with chlorine concentrations of 1, 2, and 3%, respectively. Adsorption capacities of activated carbons were determined using breakthrough curves at 140 °C. The activated carbons modified with HCl have the lowest mercury capacity. However, the difference in capacity of the differently impregnated activated carbons became progressively smaller with increasing chlorine concentration on the activated carbon. The authors suggest that the higher capacity of $CuCl_2$-impregnated activated carbon compared to that of $FeCl_3$-impregnated carbon is due to the higher electronegativity of Cu. The higher electronegativity causes a reduced electron density on the chlorine, which is therefore a stronger acceptor for the electrons of mercury. Lim et al.[31] confirmed this thesis by calculations with density functional theory (DFT).

Wang et al.[32] used six different biochars as basic materials for modification with 1 M hydrochloric acid. The materials were characterized by XPS, FTIR, and nitrogen isotherms. The adsorption capacity of modified activated carbons increased by a factor of 61 on average. It is assumed that $HgCl_2$ is formed in the micropores. In addition, the authors[15,33] modified biochar with chlorine using a nonthermal plasma, which increased the number of carbon-bound chlorine atoms. Due to this modification, a maximum of 36 times higher adsorption capacity was measured.

Shen et al.[34,35] investigated the adsorption of elemental mercury on NH_4Cl-modified biochar using breakthrough curves and XPS measurements. From the XPS analyses, it could be concluded that, in addition to chlorine atoms bound to carbon, functional oxygen groups are also involved in the chemisorption of mercury.

Using DFT, it could be shown that mercury forms chemisorptive interactions with various heteroatoms.[36,37] Wang et al.[36] investigated the effect of HCl on the adsorption of mercury on CuS surfaces using DFT. Three possible ways of HCl modification were considered: pure adsorption of HCl, the reaction of HCl and CuS to produce H_2 and H_2S, and the Deacon process. The calculations showed that the pure adsorption of HCl has no significant effect on Hg^0 adsorption. Dissociated Cl atoms, on the other hand, show a strong increase in the enthalpy of adsorption during Hg^0 adsorption. Two different adsorption mechanisms are considered. Strongly bound Cl atoms can favor the attachment of Hg to Cu atoms. Weakly bound Cl atoms favor the formation of $HgCl_2$, which is physically bound to the surface.

Chen et al.[38] proved that other heavy metals also form chemisorptive interactions with active sites on the activated carbon surface. By fitting a pseudo-second-order model to the measured data, it was shown that chemisorption is the rate-determining mechanism in adsorption.

The literature shows that impregnation of activated carbons with chlorine-containing compounds leads to a large increase in capacity for elemental mercury. However, the underlying mechanisms of elemental mercury chemisorption on chlorine-impregnated activated carbons are not understood in detail. It remains uncertain whether chemisorption predominantly involves chlorine atoms bonded to the carbon surface that form mercury−chlorine−carbon complexes or whether chlorine in the form of its compounds, which remains in the pores after impregnation and form mercuric chlorides, is the major contributor. In this work, the Chair of Thermal Process Engineering at the University of Duisburg-Essen systematically investigates the influence of the molarity of hydrochloric acid during impregnation of activated carbons on the chemisorption of mercury on different activated carbons. HCl in the pores is washed out after impregnation. Therefore, only the influence of surface bound chlorine is considered.

MATERIALS AND METHODS

Activated Carbons. As basic materials, two commercial activated carbons (AC 01 and AC 02) in the granular form with a particle diameter of 1.6−2 mm were used. Table 1 shows relevant material properties.

https://doi.org/10.1021/acsomega.2c02515
ACS Omega 2022, 7, 23833−23841

The activated carbons consist mainly of carbon with small amounts of sulfur, nitrogen, and hydrogen. Activated carbon AC 01 was produced from anthracite and has a lower oxygen content than activated carbon AC 02, which was produced from coconut shells. Both carbons were activated by steam. In a previous publication,[22] it was shown that both basic materials interact almost entirely physisorptively with mercury.

The carbons were modified by washing with 0.2, 0.6, and 1 M hydrochloric acid. For this purpose, 1 mL of hydrochloric acid (2, 6, and 10 M) was mixed with 9 mL of deionized water per 1 g of activated carbon and shaken for 3 h in a shaking incubator. The activated carbon was then washed several times with water to remove the free hydrochloric acid. The conductivity of the supernatant eluate must be <30 μS cm^{-1} after 10 h of shaking. The samples were then dried under nitrogen atmosphere in an oven at 110 °C for 12 h. Modified activated carbons are referred to as −0.2 M HCl, −0.6 M HCl, and −1 M HCl.

Characterization. A scanning electron microscope (SEM) (JSM-7500F from Jeol) and a volumetric measuring device (Autosorb iQ3 from Quantachrome Instruments) were used to characterize basic materials and modified carbons. The pore size distribution (Figure 1) was determined using quenched solid DFT (QSDFT) with a slit and cylindrical pore model.[39,40] The specific surface area was calculated using the Brunauer−Emmett−Teller (BET) method according to DIN ISO 9277. The total pore volume was determined according to the Gurvich rule at p/p_0 = 0.98, and the micropore volume by the Dubinin-Radushkevich method according to DIN 66135.[41] Table 2 shows structural properties of the adsorbents. SEM images of the carbons are illustrated in Figure 2. The surface of AC 01 consists of separate plates, while AC 02 has a fibrous structure. The different morphology is due to the different raw materials (AC 01: anthracite, AC 02: coconut shell). The nitrogen isotherms at 77 K are presented in Figure S1 in the Supporting Information. The calculated structural properties, pore size distribution, und SEM images prove that the modifications have no significant effect on the pore structure of the activated carbons.

Table 2. Structural Properties of Activated Carbons

property	AC 01	AC 01−1 M HCl	AC 02	AC 02−1 M HCl
BET-surface [$m^2 \cdot g^{-1}$]	1079	1012	951	913
total pore volume [$cm^3 \cdot g^{-1}$]	0.494	0.485	0.391	0.372
micropore volume [$cm^3 \cdot g^{-1}$]	0.387	0.379	0.376	0.332

The chlorine content of basic and modified activated carbons was determined according to DIN 51727 and DIN 10304. A distinction is made between surface-bound chlorine and chlorides, which are present in the pore structure of the activated carbon. The amount of chloride-containing salts is determined by washing the activated carbon with an absorption solution for 24 h and measuring the chloride content of the absorption solution by ion chromatography. Surface-bound chlorine can be detected by combustion of the activated carbon in oxygen atmosphere, where the surface-bound chlorine reacts to gaseous HCl. The combustion gases are passed into an alkaline absorption solution, in which HCl is captured as chloride. The chloride content of the absorption solution is determined by ion chromatography.

Experimental Approach. The experimental plant used for the adsorption and desorption experiments is shown in Figure 3. A detailed description can be found in previous publications.[26,42]

In the gas-mixing section, a defined mixture of Hg^0 (264 μg m^{-3}) and nitrogen is provided with the use of a mass flow controller. Adsorption and desorption take place in a glass vessel, in which 0.6 g of activated carbon is tempered in the range of 20−560 °C by a heating collar. The Hg^0 concentration is continuously measured using an atomic absorption spectrometer VM 3000 by Mercury Instruments GmbH. According to DIN 12846, a tin(II) chloride solution is used to reduce Hg^{2+} and Hg^+ to Hg^0. It is not possible to distinguish between Hg^{2+} and Hg^+. Therefore, this part of Hg is referred to as Hg_xCl_2 in the manuscript. Because the gas flow

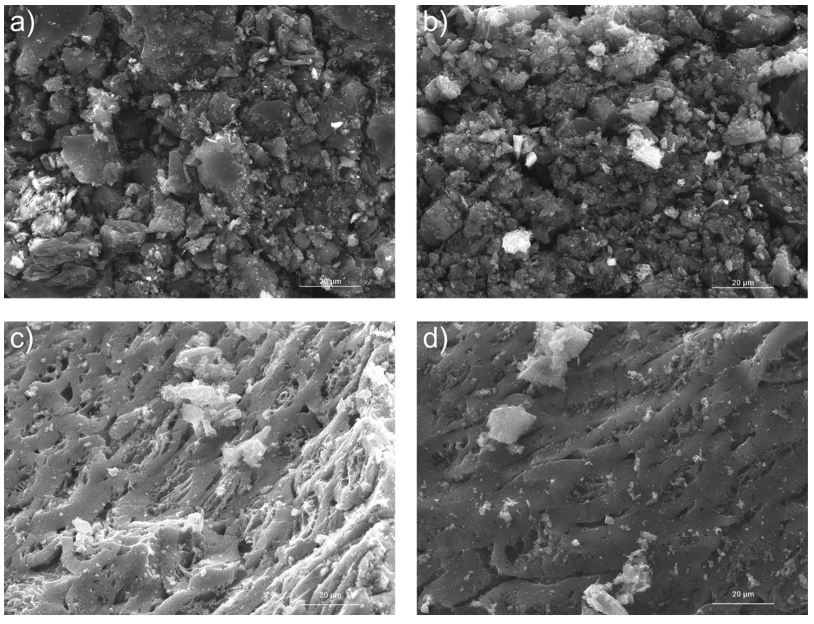

Figure 2. SEM images: (a) AC 01, (b) AC 01-1 M HCl, (c) AC 02, and (d) AC 02−1 M HCl.

https://doi.org/10.1021/acsomega.2c02515
ACS Omega 2022, 7, 23833−23841

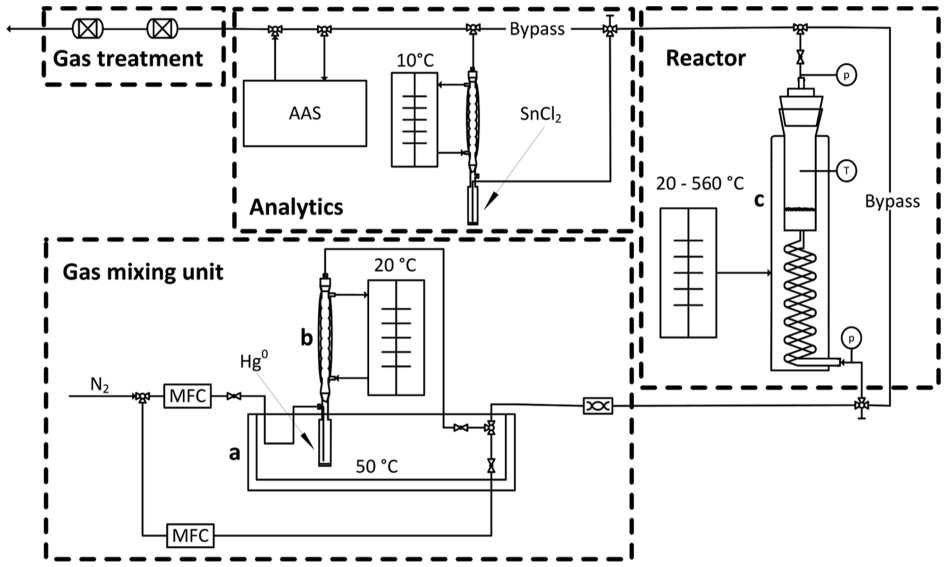

Figure 3. Schematic layout of the experimental plant, a = water bath, b = cooler, c = temperature-controlled reactor, MFC = mass flow controller, and AAS = atomic absorption spectrometer.

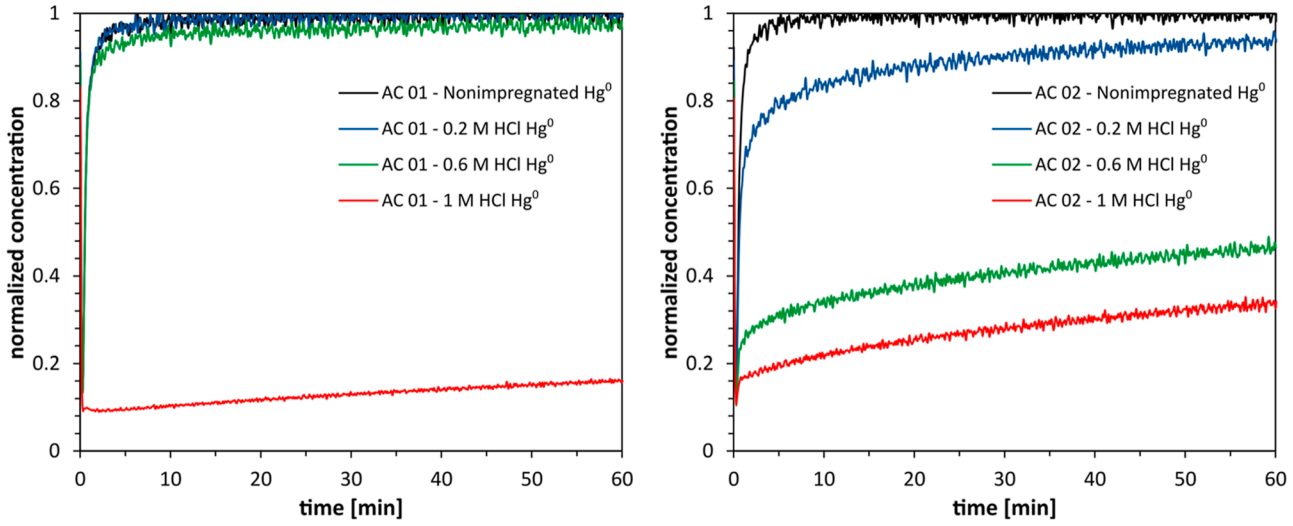

Figure 4. Breakthrough curves of Hg^0 at 100 °C with 264 $\mu g\ m^{-3}$ on the basic and HCl-modified activated carbons AC 01 (left) and AC 02 (right).

upstream of the measurement device is passed either through the tin(II) chloride solution or the bypass, a distinction is made between the Hg^0 and Hg_{total} concentrations. If the Hg^0 concentration is equal to the Hg_{total} concentration, only the Hg^0 concentration curve is shown in the diagrams below.

To investigate the chemisorption of Hg^0, coupled adsorption and desorption experiments with temperature-programmed desorption (TPD) were performed. The experiments can be divided into three sections: adsorption, concentration swing desorption (CSA), and TPD. In the adsorption part of the experiment, the mercury-containing nitrogen stream is passed over the fixed bed at a constant temperature for a defined time of 1 h. The loading of the adsorbent X_{Ads} can be calculated by integrating the area between the inlet concentration and the measured breakthrough curve. Assuming that the density of the gas is constant and only mercury is adsorbed, the global mass balance around the adsorbent yields

$$X = \frac{m_{Hg,Ads}}{m_s} = \frac{\dot{V}_{ges}}{m_s} \cdot \sum_{t=0}^{t=T} \left(\frac{c_{Hg,in} - c_{Hg,out}}{\left(1 - \frac{c_{Hg,out}}{\rho_G}\right)} \right) \cdot \Delta t_i \quad (1)$$

Here, $m_{Hg,Ads}$ is the mass of the adsorbed mercury in $\mu g\ m^{-3}$, m_s is the mass of the adsorbent in g, $\dot{V}_{ges}$ is the volume flow of the gas in L min^{-1}, c_{Hg} is the mercury concentration in $\mu g\ m^{-3}$, and ρ_G is the gas density in kg m^{-3}.

After the adsorbent has been loaded for 1 h, concentration swing desorption follows, in which the physisorptively bound mercury is desorbed. For this purpose, the adsorber is purged with pure nitrogen at the same temperature at which adsorption took place until no mercury could be detected. After that, TPD starts during which the chemisorptively bound mercury is desorbed. The temperature is continuously increased in a ramp of 5 °C min^{-1} to 560 °C. The desorbed mass of mercury during concentration swing desorption (loading X_{CSA}) and TPD (loading X_{TPD}) is calculated

https://doi.org/10.1021/acsomega.2c02515
ACS Omega 2022, 7, 23833−23841

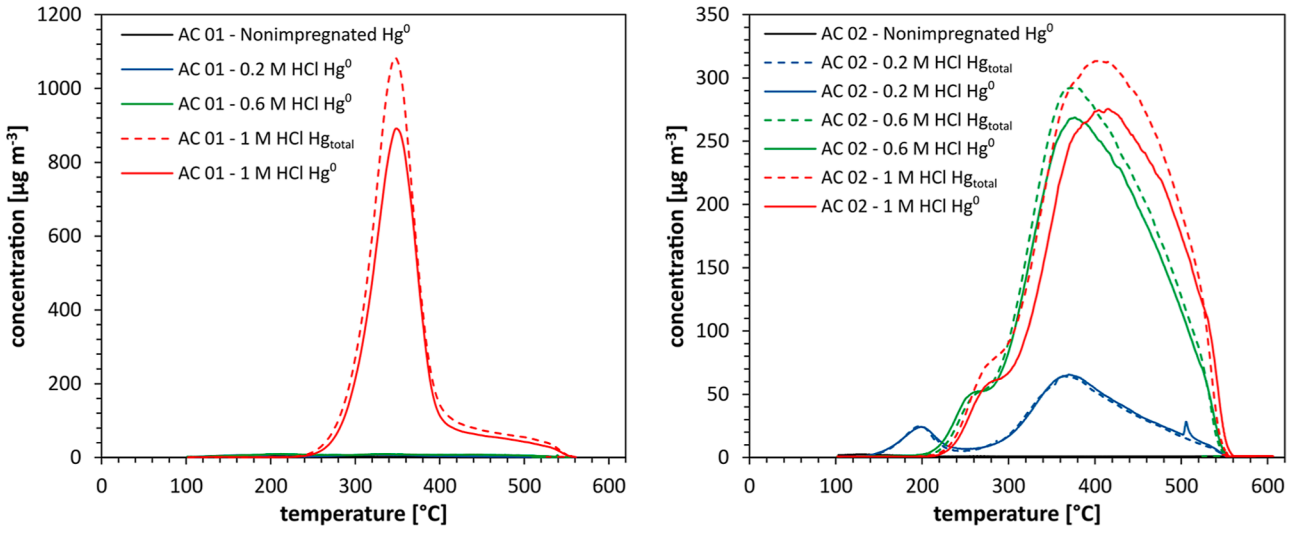

Figure 5. Hg^0 and Hg_{total} concentration curves of the TPD experiments on the basic and on the chlorine-modified activated carbons AC 01 (left) and AC 02 (right).

Table 3. Mercury Loadings and Mass Ratios of the Coupled Adsorption and Desorption Experiments of the Basic Activated Carbons and the Modified Activated Carbons AC 01 and AC 02

	loading [$\mu g\ g^{-1}$]					
activated carbon	Ads. Hg^0	CSA Hg^0	TPD Hg^0	TPD Hg_{total}	mass ratio Hg^0	mass ratio Hg_{total}
AC 01	0.254	0.149	0.097		0.97	
AC 01−0.2 M HCl	0.364	0.255	0.119		1.03	
AC 01−0.6 M HCl	2.675	0.995	1.588		0.97	
AC 01−1 M HCl	48.069	0.081	37.440	46.697	0.78	0.97
AC 02	0.237	0.204	0.038		1.02	
AC 02−0.2 M HCl	6.748	0.786	6.350		1.06	
AC 02−0.6 M HCl	32.728	0.275	28.100	31.197	0.87	0.96
AC 02−1 M HCl	38.888	0.181	30.966	36.903	0.80	0.95

according to eq 1. Then, the input concentration, $c_{Hg,in}$, corresponds to the zero line of the measuring instrument. The mass ratio of adsorption and desorption (CSA and TPD) can be calculated using eq 2.

$$\text{mass ratio} = \frac{X_{CSA} + X_{TPD}}{X_{Ads}} \cdot 100\% \quad (2)$$

RESULTS AND DISCUSSION

Dynamics of Adsorption. Figure 4 shows the Hg^0 concentration curves during elemental mercury adsorption at 100 °C for 1 h with a mercury concentration of 264 $\mu g\ m^{-3}$ on the basic activated carbons and the HCl-modified activated carbons AC 01 (left) and AC 02 (right).

The Hg^0 concentration curves of the adsorption for 1 h are identical to the Hg_{total} concentration curves in all experiments, no Hg^{2+} or Hg^+ (e.g., in the form of Hg_xCl_2) was detected. The Hg^0 concentration curves of the basic activated carbons have an early breakthrough and a rapid increase in concentration. After about 15 min, a state of equilibrium is reached, in which the input concentration equals the output concentration. The concentration curves of activated carbons AC 01 modified with 0.2 M and 0.6 M HCl are identical to the concentration curve for the basic activated carbon. The activated carbon AC 01 treated with 1 M HCl also has an initial breakthrough, followed by a very slow increase in concentration, so that no equilibrium state is reached after the specified experimental time. The very slow kinetics and the high capacity of adsorption indicate chemisorptive interactions between Hg^0 and the activated carbon surface.

The concentration curves of the modified activated carbons AC 02 have an initial breakthrough, followed by a very slow increase in concentration. The capacities of these activated carbons increase with the molarity of the hydrochloric acid used during the preparation. The concentration curves of all modified activated carbons AC 02 also indicate a chemisorptive adsorption mechanism with slow kinetics and high capacity.

Temperature-Programmed Desorption of Mercury. For a detailed study of mechanisms involved, coupled adsorption and desorption experiments were performed with CSA and TPD. For this purpose, 0.6 g of the activated carbon was first loaded with a mercury concentration of 264 $\mu g\ m^{-3}$ at 100 °C for 1 h. Subsequently, physisorptively bound mercury was desorbed by CSA, and chemisorptively bound mercury was desorbed by continuously increasing the temperature in a ramp function of 5 °C min^{-1} (TPD). Figure 5 shows the Hg^0 and Hg_{total} concentration curves of the TPD experiments on the basic and the chlorine-modified activated carbons AC 01 (left) and AC 02 (right).

Table 3 shows the loadings and mass ratios of the coupled adsorption and desorption experiments with CSA and TPD. The concentration curves for Hg^0 and Hg_{total} are identical for all adsorption and CSA measurements.

https://doi.org/10.1021/acsomega.2c02515
ACS Omega 2022, 7, 23833−23841

The maximum concentrations of the two basic activated carbons and the activated carbon AC 01 modified with 0.2 and 0.6 M HCl are very low because hardly any chemisorptively bound mercury is present (Table 3). The desorption curves for Hg^0 and Hg_{total} of activated carbon AC 01 treated with 1 M HCl (Figure 5, left) have two peaks with maximum concentrations at temperatures of 350 and 480 °C, respectively. The curves for Hg^0 and Hg_{total} are almost identical, with the Hg^0 concentration consistently below the Hg_{total} concentration. From the difference, it can be concluded that Hg^{2+} or Hg^+ — in the form of Hg_xCl_2 — forms and desorbs during TPD. The temperature interval, in which Hg_xCl_2 desorbs is identical to the temperature interval, in which Hg^0 desorbs. It is also evident by the coupled adsorption and desorption curves that Hg_xCl_2 formed is exclusively from the desorption of mercury chemisorptively bound to the activated carbon. No physisorptively bound Hg_xCl_2 is detected in the experiments. The calculated mass ratios of Hg^0 and Hg_{total} suggest that about 20% of the chemisorptively bound mercury desorbs in the form of Hg_xCl_2. The chemisorptively bound mercury is thermally stable up to a temperature of 240 °C. The TPD concentration curves show that two different chemisorptive adsorption mechanisms are present, whose reaction products desorb at different temperatures and therefore have different bonding strengths to the surface. Comparing the chemisorptive loadings of the AC 01-activated carbon with the chlorine content of the activated carbons (Table 4), it is concluded that surface-bound chlorine must be present for significant chemisorption of mercury. It is assumed that mercury−chlorine surface complexes with different energetic values are formed.

The concentration curves of activated carbon AC 02 modified with HCl (Figure 5 right) also show two peaks. The desorption peaks of activated carbon treated with 0.2 M HCl are the smallest. More mercury is chemisorptively bound on AC 02 treated with 0.6 and 1 M HCl (Table 3). Maximum concentrations are reached at temperatures of 260 and 360 °C for the activated carbon modified with 0.6 M HCl. The concentration curves of the carbon modified with 1 M HCl are similar to those of the carbon modified with 0.6 M HCl. However, the maximum concentrations are shifted to about 15 °C higher temperatures. From the concentration curves of Hg^0 and Hg_{total}, it is evident that only in the case of the carbon modified with 0.6 M HCl and 1 M HCl, Hg_xCl_2 is formed during desorption. This Hg_xCl_2 formed on the surface of the activated carbon is exclusively chemisorptively bound, which could also be observed in the experiments with AC 01. The percentage of mercury in the form of Hg_xCl_2 is about 13% on AC 02 treated with 0.6 M HCl and about 20% on AC 02 treated with 1 M HCl (Table 3). The mass of chemisorptively bound mercury also correlates with surface-bound chlorine for activated carbon AC 02 (Table 4). The concentration curves of AC 02 modified with 0.6 M HCl and 1 M HCl also show two Hg bonding mechanisms with products of different energetic values. The bound mercury is thermally stable up to 220 °C in these activated carbons. AC 02 treated with 0.2 M HCl is the only activated carbon that shows significant chemisorption of mercury, although no surface-bound chlorine is present (Table 4). It is suggested that the increase in capacity here is due to an accumulation of mercury on oxygen functional groups formed or exposed during modification of the carbons. This mechanism has been proposed in a previous publication[27] and could also provide a small contribution to chemisorption of mercury in other modified materials. Compared to the loadings found in this work, the loadings described in ref.[27] are significantly lower.

Table 4. Chlorine and the Chloride Content of the Adsorbents in Mass % of Dry Mass (m % dm)

activated carbon	Cl on surface [m % dm]	Cl^- in salts [m % dm]
AC 01	0.024	0.005
AC 01−0.2 M HCl	0.036	0.005
AC 01−0.6 M HCl	0.026	0.005
AC 01−1 M HCl	0.690	0.005
AC 02	0.051	0.050
AC 02−0.2 M HCl	0.037	0.008
AC 02−0.6 M HCl	0.130	0.006
AC 02−1 M HCl	0.510	0.004

Table 4 shows the chlorine content of the basic activated carbons and the modified activated carbons AC 01 and AC 02 with chlorine bound on the surface and chloride in salts in the pores.

The mass fraction of chloride containing salts present in the pore structure is very low for all activated carbons with a maximum value of 0.05 m % dm. The proportion of surface-bound chlorine is of a similar order of magnitude for the basic AC 01 and the AC 01 treated with 0.2 and 0.6 M HCl and increases significantly only after modification with 1 M HCl. For the basic AC 02 and the AC 02 modified with 0.2 M HCl, the mass fraction of chlorine on the surface is low. The coal AC 02 treated with 0.6 M HCl and 1 M HCl show a significant increase in surface-bound chlorine compared to the basic material. A mechanism for the attachment of chlorine in the aqueous phase is proposed in the literature.[43,44] During modification of activated carbon, hydrochloric acid dissociates and a hydrogen ion protonates, for example, a carbonyl group of a pyrone group. The positive charge is shifted to the ether oxygen by mesomeric stabilization, and the chloride ion stabilizes the positive charge as a counter ion. During drying of the activated carbons, the chloride ion deposits on the surface. The kinetics of this mechanism have not been investigated. Therefore, it cannot be conclusively explained why the activated carbon AC 01 shows an increase in surface-bound chlorine only after treatment with 1 M HCl, while surface-bound chlorine is detected in the activated carbon AC 02 already after treatment with 0.6 M HCl. The results of the elemental analyses were verified by replicate measurements.

To further investigate the mechanisms, experiments were performed with a variation of the adsorbent mass. In the coupled adsorption and desorption experiments, 0.6 and 6 g activated carbon were used. Figure 6 shows the concentration curves of the TPD experiments on AC 01 (left) and AC 02 (right) modified with 1 M HCl.

Loadings and mass ratios of the experiments with variation of adsorbent mass are shown in Table 5. Only the Hg^0 value is given for the adsorption and CSA loadings, and no Hg^{2+} or Hg^+ was detected.

The TPD concentration curves of the experiments with 6 g activated carbon have a different peak geometry compared to the concentration curves of the experiments with 0.6 g activated carbon, and desorption takes place at higher temperatures. The adsorption experiments (Figure 4) showed that the carbons treated with 1 M HCl have a very high capacity for elemental mercury. Experiments with an adsorption temperature of 260 °C (Supporting Information

https://doi.org/10.1021/acsomega.2c02515
ACS Omega 2022, 7, 23833−23841

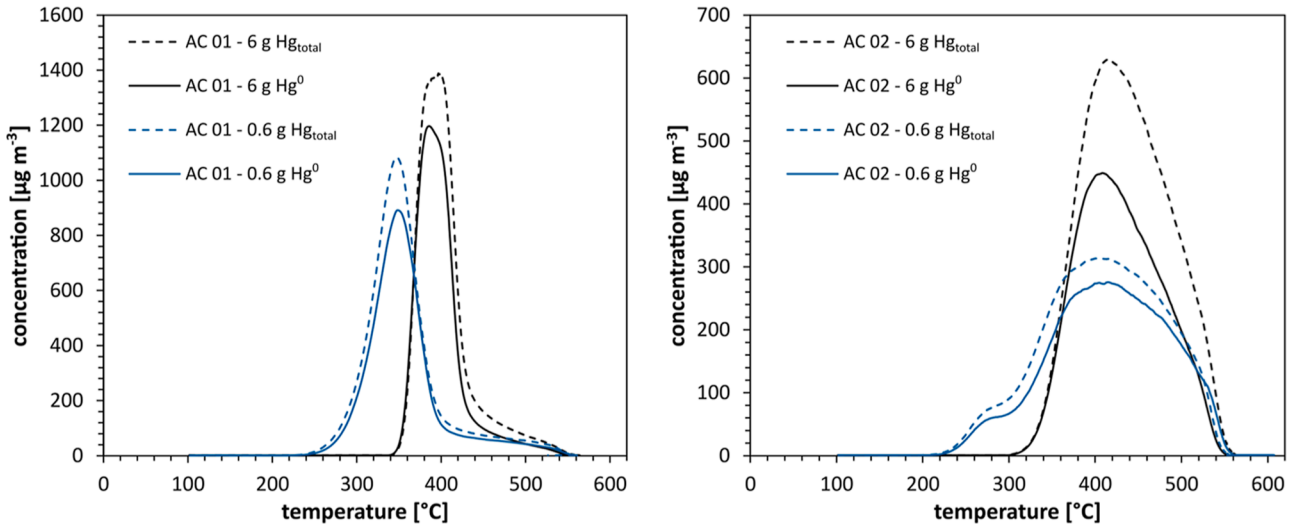

Figure 6. Hg^0 and Hg_{total} concentrations of the TPD experiments with 6 and 0.6 g activated carbons treated with 1 M HCl, AC 01 (left) and AC 02 (right).

Table 5. Mercury Loadings and Mass Ratios of Coupled Adsorption and Desorption Experiments with 6 and 0.6 g Activated Carbon

		loading [$\mu g\ g^{-1}$]					
activated carbon	mass [g]	ads. Hg^0	CSA Hg^0	TPD Hg^0	TPD Hg_{total}	mass ratio Hg^0	mass ratio Hg_{total}
AC 01−1 M HCl	0.6	48.069	0.081	37.440	46.697	0.78	0.97
	6	5.194	0.053	3.754	4.825	0.73	0.94
AC 02−1 M HCl	0.6	38.888	0.181	30.966	36.903	0.80	0.95
	6	5.447	0.003	3.482	5.171	0.64	0.95

Figure S2) demonstrated that mercury is still chemisorptively bound to the carbon even at very high temperatures. Therefore, the changed peak geometry and the shift of the desorption peaks to higher temperatures in the experiments with 6 g activated carbon are probably due to readsorption effects. Mercury is desorbed in the front part of the fixed bed with 6 g activated carbon and passes to unloaded activated carbon in the upper part of the bed, where it is adsorbed again. This effect leads to a shift of desorption peaks to higher temperatures and higher maximum concentrations. In the experiments with 0.6 g activated carbon, readsorption effects can be neglected due to the shorter activated carbon bed.

The reduction of the adsorbent mass leads to a significant increase in the loading of the activated carbons (Table 5) because an identical amount of mercury is passed over the fixed bed during adsorption, and the adsorbent mass is lower. The ratio of adsorptively bound mercury to surface-bound chlorine atoms is shifted in favor of the bound mercury in the experiments with 0.6 g activated carbon. As a result, the Hg^0 mass ratio of adsorbed to desorbed mercury increases significantly in experiments with lower adsorbent mass. Consequently, a higher loading of mercury on the activated carbon yields less Hg_xCl_2. This tendency is confirmed by experiments with variation of the loading duration (Supporting Information Figure S3 and Table S1). A proposed mechanistic explanation for this effect is shown in Figure 7.

During adsorption, mercury from the gas phase forms surface complexes with chlorine atoms. The distinct Hg^0 desorption peaks probably result from decomposition of surface complexes of one Hg^0 atom and one surface-bonded chlorine atom. Formation of $HgCl_2$, on the other hand, could

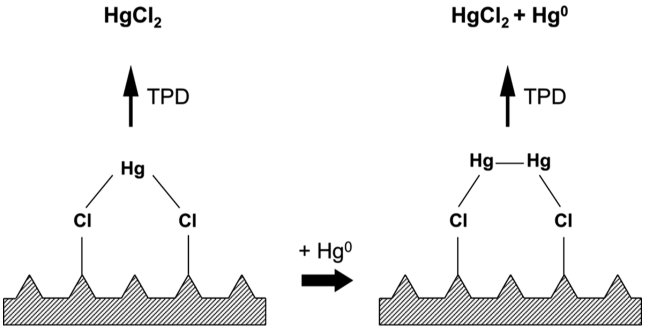

Figure 7. Proposed reaction sequence for the formation of $HgCl_2$ and Hg^0 during TPD after chemisorption of Hg^0 to surface-bound chlorine.

be due to interactions of one Hg^0 atom with two surface-bonded chlorine atoms (Figure 7 left). This complex decomposes to $HgCl_2$ during TPD. A higher loading of mercury on activated carbon may result in a further addition of Hg^0 from the gas phase to the existing $HgCl_2$ complex (Figure 7 right). This new complex decomposes to $HgCl_2$ and Hg^0 during TPD. Klöfer et al.[45] examined the gaseous products released during heating of solid $HgCl_2$ and solid Hg_2Cl_2. When solid $HgCl_2$ is heated, only $HgCl_2$ is present in the gas phase. In contrast, when solid Hg_2Cl_2 is heated, both $HgCl_2$ and Hg^0 are present in the gas phase. Because Hg^0 is formed in the gas phase during decomposition of Hg_2Cl_2, this step may be an explanation for the higher Hg^0 mass ratio at higher loadings. These results support the assumptions described above about rearrangement and subsequent decomposition of surface complexes in Figure 7. It must be emphasized that this

https://doi.org/10.1021/acsomega.2c02515
ACS Omega 2022, 7, 23833−23841

mechanistic discussion of Hg^0 chemisorption is speculative and sketchy. However, it can be assumed that mercury forms two covalent bonds. In corresponding complexes, mercury has oxidation numbers +1 and +2, respectively, as in many known mercury compounds. The complexes in Figure 7 meet these conditions. The attachment of chlorine atoms to the surface of activated carbon has already been described in detail in the previous paragraphs, and is only shown schematically in Figure 7.

CONCLUSIONS

The influence of chlorine on the adsorption of mercury was investigated by measuring breakthrough curves and by TPD experiments. Two activated carbons were used as basic materials and modified with 0.2, 0.6, and 1 M HCl. Elemental analyses proved that only surface-bound chlorine is present after modification of AC 01 with 1 M HCl and AC 02 with 0.6 and 1 M HCl. Coupled adsorption and desorption experiments with TPD showed that mercury forms surface complexes with chlorine, greatly increasing the chemisorptive capacity of the carbons. The detection of several desorption peaks at different desorption temperatures suggests different chemisorptive mechanisms with mercury and surface-bound chlorine. The influence of hydrochloric acid remaining in the pores after modification can be excluded in all experiments due to thorough washing.

Measurements of the concentration of Hg^0 and Hg_{total} showed that during the desorption of mercury from the surface of the modified activated carbons, Hg_xCl_2 is formed. On the contrary, $HgCl_2$ (s) as a solid compound in the pores can be excluded because no HCl is available in the pores. Experiments with a variation in adsorbent mass showed that the fraction of Hg_xCl_2 depends on the mercury loading of the activated carbon, with a maximum mass fraction of 27% of Hg in Hg_xCl_2. A mechanistic proposal describes the conversion of a bound $HgCl_2$ complex by incorporation of a Hg atom into a Hg_2Cl_2 complex at higher mercury loadings.

The complex process of mercury chemisorption on different surface-bound heteroatoms should be studied in detail in subsequent work. For this purpose, the surface of activated carbons should be systematically modified by chemical reactions. The base materials and the modified materials can then be used to study the mechanisms of adsorption and desorption of mercury. The characterization of the materials should be based on different measurement methods such as volumetric measurements of nitrogen isotherms, Boehm titration, SEM, or XPS. Especially, XPS measurements could help to detect different mercury species on the surface of the materials.

ASSOCIATED CONTENT

Supporting Information

The Supporting Information is available free of charge at https://pubs.acs.org/doi/10.1021/acsomega.2c02515.

Nitrogen isotherms; mercury adsorption at 260 °C and TPD; influence of the loading duration (PDF)

AUTHOR INFORMATION

Corresponding Author

Julian Steinhaus − *Chair of Thermal Process Engineering, University of Duisburg-Essen, D-47057 Duisburg, Germany;* orcid.org/0000-0002-5621-8186; Email: julian.steinhaus@uni-due.de

Authors

Christoph Pasel − *Chair of Thermal Process Engineering, University of Duisburg-Essen, D-47057 Duisburg, Germany*

Christian Bläker − *Chair of Thermal Process Engineering, University of Duisburg-Essen, D-47057 Duisburg, Germany*

Dieter Bathen − *Chair of Thermal Process Engineering, University of Duisburg-Essen, D-47057 Duisburg, Germany; Institute of Energy and Environmental Technology, IUTA e. V., D-47229 Duisburg, Germany*

Complete contact information is available at: https://pubs.acs.org/10.1021/acsomega.2c02515

Notes

The authors declare no competing financial interest.

ACKNOWLEDGMENTS

This work was funded by Deutsche Forschungsgemeinschaft (DFG). We acknowledge support by the Open Access Publication Fund of University of Duisburg-Essen. The activated carbons were kindly provided by Carbon Service & Consulting GmbH & Co KG.

REFERENCES

(1) Wang, Y.; Liu, Y.; Wu, Z.; Mo, J.; Cheng, B.; Cheng, B. Experimental study on the absorption behaviors of gas phase bivalent mercury in Ca-based wet flue gas desulfurization slurry system. *J. Hazard. Mater.* **2010**, *183*, 902−907.

(2) Krzyżyńska, R.; Szeliga, Z.; Pilar, L.; Borovec, K.; Regucki, P. High mercury emission (both forms: Hg^0 and Hg^{2+}) from the wet scrubber in a full-scale lignite-fired power plant. *Fuel* **2020**, *270*, 117491.

(3) Xu, J.; Bao, J.; Tang, J.; Du, M.; Liu, H.; Xie, G.; Yang, H. Characteristics and Inhibition of Hg^0 Re-emission in a Wet Flue Gas Desulfurization System. *Energy Fuels* **2018**, *32*, 6111−6118.

(4) Zhou, Q.; Duan, Y.-F.; Zhu, C.; She, M.; Zhang, J.; Yao, T. In-Flight Mercury Removal and Cobenefit of SO_2 and NO Reduction by NH_4Br Impregnated Activated Carbon Injection in an Entrained Flow Reactor. *Energy Fuels* **2015**, *29*, 8118−8125.

(5) Zhang, Y.; Zhao, L.; Guo, R.; Song, N.; Wang, J.; Cao, Y.; Orndorff, W.; Pan, W.-P. Mercury adsorption characteristics of HBr-modified fly ash in an entrained-flow reactor. *J. Environ. Sci.* **2015**, *33*, 156−162.

(6) Zhang, Y.; Duan, W.; Liu, Z.; Cao, Y. Effects of modified fly ash on mercury adsorption ability in an entrained-flow reactor. *Fuel* **2014**, *128*, 274−280.

(7) Serre, S. D.; Gullett, B. K.; Ghorishi, S. B. Entrained-flow adsorption of mercury using activated carbon. *J. Air Waste Manage. Assoc.* **2001**, *51*, 733−741.

(8) Hsi, H.-C.; Tsai, C.-Y.; Lin, K.-J. Impact of Surface Functional Groups, Water Vapor, and Flue Gas Components on Mercury Adsorption and Oxidation by Sulfur-Impregnated Activated Carbons. *Energy Fuels* **2014**, *28*, 3300−3309.

(9) Tan, Z.; Sun, L.; Xiang, J.; Zeng, H.; Liu, Z.; Hu, S.; Qiu, J. Gas-phase elemental mercury removal by novel carbon-based sorbents. *Carbon* **2012**, *50*, 362−371.

(10) Hsi, H.-C.; Chen, C.-T. Influences of acidic/oxidizing gases on elemental mercury adsorption equilibrium and kinetics of sulfur-impregnated activated carbon. *Fuel* **2012**, *98*, 229−235.

(11) Olson, E. S.; Miller, S. J.; Sharma, R. K.; Dunham, G. E.; Benson, S. A. Catalytic effects of carbon sorbents for mercury capture. *J. Hazard. Mater.* **2000**, *74*, 61−79.

(12) Sano, A.; Takaoka, M.; Shiota, K. Vapor-phase elemental mercury adsorption by activated carbon co-impregnated with sulfur and chlorine. *Chem. Eng. J.* **2017**, *315*, 598−607.
(13) Chen, Y.; Guo, X.; Wu, F.; Huang, Y.; Yin, Z. Experimental and theoretical studies for the mechanism of mercury oxidation over chlorine and cupric impregnated activated carbon. *Appl. Surf. Sci.* **2018**, *458*, 790−799.
(14) Jang, H.-N.; Back, S.-K.; Sung, J.-H.; Jeong, B.-M.; Kang, Y.-S.; Lee, C.-K.; Jurng, J.; Seo, Y.-C. Adsorption and kinetics of elemental mercury vapor on activated carbons impregnated with potassium iodide, hydrogen chloride, and sulfur. *Korean J. Chem. Eng.* **2017**, *34*, 806−813.
(15) Zhang, H.; Wang, T.; Sui, Z.; Zhang, Y.; Norris, P.; Sun, B.; Pan, W.-P. Plasma Induced Addition of Active Functional Groups to Biochar for Elemental Mercury Removal. *Plasma Chem. Plasma Process.* **2019**, *39*, 1449−1468.
(16) He, P.; Zhang, X.; Peng, X.; Jiang, X.; Wu, J.; Chen, N. Interaction of elemental mercury with defective carbonaceous cluster. *J. Hazard. Mater.* **2015**, *300*, 289−297.
(17) Karatza, D.; Lancia, A.; Prisciandaro, M.; Musmarra, D.; Mazziotti di Celso, G. Influence of oxygen on adsorption of elemental mercury vapors onto activated carbon. *Fuel* **2013**, *111*, 485−491.
(18) Musmarra, D.; Karatza, D.; Lancia, A.; Prisciandaro, M.; Mazziotti, G.; Di Mazziotti Celso, G. A Comparison among Different Sorbents for Mercury Adsorption from Flue Gas. *Chem. Eng. Trans.* **2015**, *43*, 2461.
(19) Skodras, G.; Diamantopoulou, I.; Pantoleontos, G.; Sakellaropoulos, G. P. Kinetic studies of elemental mercury adsorption in activated carbon fixed bed reactor. *J. Hazard. Mater.* **2008**, *158*, 1−13.
(20) Diamantopoulou, I.; Skodras, G.; Sakellaropoulos, G. P. Sorption of mercury by activated carbon in the presence of flue gas components. *Fuel Process. Technol.* **2010**, *91*, 158−163.
(21) Ambrosy, J. M.; Steinhaus, J.; Pasel, C.; Bläker, C.; Bittig, M.; Bathen, D. Simulative Investigation of the Application of Non-impregnated Activated Carbon in a Multilayer Adsorber for the Separation of Hg^0 from Discontinuous Waste Gas Streams. *Ind. Eng. Chem. Res.* **2021**, *60*, 4097.
(22) Ambrosy, J. M.; Pasel, C.; Luckas, M.; Bittig, M.; Bathen, D. A Detailed Investigation of Adsorption Isotherms, Enthalpies, and Kinetics of Mercury Adsorption on Nonimpregnated Activated Carbon. *Ind. Eng. Chem. Res.* **2019**, *58*, 4208−4221.
(23) Karatza, D.; Prisciandaro, M.; Lancia, A.; Musmarra, D. Silver impregnated carbon for adsorption and desorption of elemental mercury vapors. *J. Environ. Sci.* **2011**, *23*, 1578−1584.
(24) Skodras, G.; Diamantopoulou, I.; Zabaniotou, A.; Stavropoulos, G.; Sakellaropoulos, G. P. Enhanced mercury adsorption in activated carbons from biomass materials and waste tires. *Fuel Process. Technol.* **2007**, *88*, 749−758.
(25) Liu, J.; Cheney, M. A.; Wu, F.; Li, M. Effects of chemical functional groups on elemental mercury adsorption on carbonaceous surfaces. *J. Hazard. Mater.* **2011**, *186*, 108−113.
(26) Ambrosy, J. M.; Pasel, C.; Luckas, M.; Bittig, M.; Bathen, D. Influence of Oxygen on Hg^0 Adsorption on Non-Impregnated Activated Carbons. *ACS Omega* **2020**, *5*, 17051−17061.
(27) Steinhaus, J.; Pasel, C.; Bläker, C.; Bathen, D. Impact of H_2O on the Adsorption of Hg^0 on Activated Carbon. *ACS Omega* **2021**, *6*, 16989−17001.
(28) Zeng, H.; Jin, F.; Guo, J. Removal of elemental mercury from coal combustion flue gas by chloride-impregnated activated carbon. *Fuel* **2004**, *83*, 143−146.
(29) Lee, S. J.; Seo, Y.-C.; Jurng, J.; Lee, T. G. Removal of gas-phase elemental mercury by iodine- and chlorine-impregnated activated carbons. *Atmos. Environ.* **2004**, *38*, 4887−4893.
(30) Choi, S.; Lee, S.-S. Mercury adsorption characteristics of Cl-impregnated activated carbons in simulated flue gases. *Fuel* **2021**, *299*, 120822.
(31) Lim, D.-H.; Choi, S.; Park, J.; Senthamaraikannan, T. G.; Min, Y.; Lee, S.-S. Fundamental Mechanisms of Mercury Removal by $FeCl_3$ - and $CuCl_2$ -Impregnated Activated Carbons: Experimental and First-Principles Study. *Energy Fuels* **2020**, *34*, 16401−16410.
(32) Wang, T.; Wu, J.; Zhang, Y.; Liu, J.; Sui, Z.; Zhang, H.; Chen, W.-Y.; Norris, P.; Pan, W.-P. Increasing the chlorine active sites in the micropores of biochar for improved mercury adsorption. *Fuel* **2018**, *229*, 60−67.
(33) Wang, T.; Liu, J.; Zhang, Y.; Zhang, H.; Chen, W.-Y.; Norris, P.; Pan, W.-P. Use of a non-thermal plasma technique to increase the number of chlorine active sites on biochar for improved mercury removal. *Chem. Eng. J.* **2018**, *331*, 536−544.
(34) Shen, B.; Tian, L.; Li, F.; Zhang, X.; Xu, H.; Singh, S. Elemental mercury removal by the modified bio-char from waste tea. *Fuel* **2017**, *187*, 189−196.
(35) Li, G.; Shen, B.; Li, Y.; Zhao, B.; Wang, F.; He, C.; Wang, Y.; Zhang, M. Removal of element mercury by medicine residue derived biochars in presence of various gas compositions. *J. Hazard. Mater.* **2015**, *298*, 162−169.
(36) Wang, Y.; Huo, Q.; Shi, L.; Feng, G.; Wang, J.; Han, L.; Chang, L. Adsorption of mercury species on selected CuS surfaces and the effects of HCl. *Chem. Eng. J.* **2020**, *393*, 124773.
(37) Geng, L.; Han, L.; Cen, W.; Wang, J.; Chang, L.; Kong, D.; Feng, G. A first-principles study of Hg adsorption on Pd(1 1 1) and Pd/γ-Al2O3(1 1 0) surfaces. *Appl. Surf. Sci.* **2014**, *321*, 30−37.
(38) Chen, Y.; Chen, J.; Chen, S.; Tian, K.; Jiang, H. Ultra-high capacity and selective immobilization of Pb through crystal growth of hydroxypyromorphite on amino-functionalized hydrochar. *J. Mater. Chem. A* **2015**, *3*, 9843.
(39) Neimark, A. V.; Lin, Y.; Ravikovitch, P. I.; Thommes, M. Quenched solid density functional theory and pore size analysis of micro-mesoporous carbons. *Carbon* **2009**, *47*, 1617−1628.
(40) Bläker, C.; Muthmann, J.; Pasel, C.; Bathen, D. Characterization of Activated Carbon Adsorbents − State of the Art and Novel Approaches. *ChemBioEng Rev.* **2019**, *6*, 119−138.
(41) Haul, R.; Gregg, S. J.; Sing, K. S. W. Adsorption, Surface Area and Porosity. *Berichte der Bunsengesellschaft für physikalische Chemie*, 2nd ed.; Academic Press: London, 1982.
(42) Ambrosy, J.; Pasel, C.; Luckas, M.; Bittig, M.; Bathen, D. Comprehensive Methodology for the Investigation of Mercury Adsorption on Activated Carbons. *Chem. Ing. Tech.* **2019**, *91*, 1874−1884.
(43) Boehm, H. P. Some aspects of the surface chemistry of carbon blacks and other carbons. *Carbon* **1994**, *32*, 759−769.
(44) Boehm, H.-P. Surface chemical characterization of carbons from adsorption studies. *Adsorption by Carbons*; Elsevier: Amsterdam, 2008.
(45) Klöfer, I.; Bittig, M.; Bathen, D. Speciation of Inorganic Mercury Compounds in Solid Samples via Thermo-desorption Experiments. *Chem. Eng. Technol.* **2021**, *44*, 788−796.

https://doi.org/10.1021/acsomega.2c02515
ACS Omega 2022, 7, 23833−23841